AD-A077 907 AIR FORCE GEOPHYSICS LAB HANSCOM AFB MA F/G 4/1
SPACECRAFT CHARGING MODEL - TWO MAXWELLIAN APPROXIMATION.(U)
JUL 79 P TSIPOURAS , H B GARRETT
UNCLASSIFIED AFGL-TR-79-0153 NL

| OF |
AD A077907

END
DATE FILMED
1-80
DDC

AFGL-TR-79-0153
ENVIRONMENTAL RESEARCH PAPERS, NO. 667

Spacecraft Charging Model—Two Maxwellian Approximation

P. TSIPOURAS
H. B. GARRETT, Capt, USAF

13 July 1979

SPACE PHYSICS DIVISION PROJECT 7661

AIR FORCE GEOPHYSICS LABORATORY
HANSCOM AFB, MASSACHUSETTS 01731

AIR FORCE SYSTEMS COMMAND, USAF

Unclassified

SECURITY CLASSIFICATION OF THIS PAGE (When Data Entered)

REPORT DOCUMENTATION PAGE	READ INSTRUCTIONS BEFORE COMPLETING FORM
1. REPORT NUMBER: AFGL-TR-79-0153 (AFGL-ERP-667)	2. GOVT ACCESSION NO. / 3. RECIPIENT'S CATALOG NUMBER
4. TITLE (and Subtitle): SPACECRAFT CHARGING MODEL – TWO MAXWELLIAN APPROXIMATION	5. TYPE OF REPORT & PERIOD COVERED: Scientific. Interim.
	6. PERFORMING ORG. REPORT NUMBER: ERP No. 667
7. AUTHOR(s): P. Tsipouras, H. B. Garrett, Capt. USAF	8. CONTRACT OR GRANT NUMBER(s)
9. PERFORMING ORGANIZATION NAME AND ADDRESS: Air Force Geophysics Laboratory (PHG), Hanscom AFB, Massachusetts 01731	10. PROGRAM ELEMENT, PROJECT, TASK AREA & WORK UNIT NUMBERS: 62101F, 76610803
11. CONTROLLING OFFICE NAME AND ADDRESS: Air Force Geophysics Laboratory (PHG), Hanscom AFB, Massachusetts 01731	12. REPORT DATE: 13 July 1979 / 13. NUMBER OF PAGES: 28
14. MONITORING AGENCY NAME & ADDRESS (if different from Controlling Office)	15. SECURITY CLASS. (of this report): Unclassified / 15a. DECLASSIFICATION/DOWNGRADING SCHEDULE

16. DISTRIBUTION STATEMENT (of this Report)

Approved for public release; distribution unlimited.

17. DISTRIBUTION STATEMENT (of the abstract entered in Block 20, if different from Report)

Environmental research papers

18. SUPPLEMENTARY NOTES

19. KEY WORDS (Continue on reverse side if necessary and identify by block number)

Spacecraft charging
Geosynchronous modeling
Charge modeling

20. ABSTRACT (Continue on reverse side if necessary and identify by block number)

The ambient plasma environment at geosynchronous orbit is assumed to be represented by a two-component Maxwell-Boltzmann particle distribution. Given this, the equations for ambient electron and ion currents to the spacecraft are easily integrated. Likewise, the secondary and backscattered currents can be expressed as integrals. The potential at which the currents balance gives the potential between the spacecraft and ambient plasma. The model is compared with actual data from ATS-5 and is found to agree within

over

DD FORM 1 JAN 73 1473 EDITION OF 1 NOV 65 IS OBSOLETE

Unclassified

SECURITY CLASSIFICATION OF THIS PAGE (When Data Entered)

409 578

PLUS OR MINUS

MINUS

20. Abstract (Continued)

±1, 200 V over a range of 0 to -10, 000 V. The model is readily applicable to the simple environmental model of Garrett and DeForest (1979) and can be calibrated to any given satellite. Simple algorithmic expressions are also developed for the backscattered and secondary currents as a function of temperature and potential which promise a significant decrease in computer time without a significant loss in accuracy.

Preface

This paper grew out of discussions with S. E. DeForest, E.C. Whipple, A. Rubin, and L.W. Parker. The data were provided by UCSD (S.E. DeForest). C.P. Pike provided extensive encouragement.

Contents

Illustrations

Illustrations

Table

Spacecraft Charging Model– Two Maxwellian Approximation

1. INTRODUCTION

In Garrett[1] and Garrett and DeForest,[2] it was demonstrated that the plasma at geosynchronous orbit is to first order representable by expansions in terms of Maxwellian distributions. In particular, a description in terms of the sum of two Maxwellian components was found to adequately represent the plasma in about 80 percent of the cases studied. In Garrett,[3] a simple spacecraft charging code based on the work of Whipple[4] and DeForest[5] was developed which made use of the discrete particle measurements returned by the ATS-5 geosynchronous satellite in the energy range 50 eV to 50 keV. The model suffered, however, from being unable to treat accurately Maxwellian components except in a narrow range of potentials and temperatures due to the necessity of taking discrete energy steps

(Received for publication 12 July 1979)

1. Garrett, H.B. (1977) Modeling of the Geosynchronous Orbit Plasma Environment – Part I, AFGL-TR-77-0288, AD A053 164.
2. Garrett, H.B. and DeForest, S.E. (1979b) An analytical simulation of the geosynchronous plasma environment. to appear in Planet. Space Sci.
3. Garrett, H.B. (1978) Spacecraft Potential Calculations – A Model, AFGL-TR-78-0116, AF Surveys in Geophysics, No. 387, AD A060 151.
4. Whipple, E.C. (1965) The Equilibrium Electric Potential of a Body in the Upper Atmosphere, NASA X-615-65-296.
5. DeForest, S.E. (1972) Spacecraft charging at synchronous orbit, J. Geophys. Res. 27:651.

in performing integrations (that is, a temperature of 10 eV would require at least 1 eV resolution; a temperature of 20 keV would then require over 40,000 such steps if both were to be resolved simultaneously). It became clear that the only solution to such a problem was to carry out the detailed calculation of the currents associated with a Maxwellian distribution function.

In the first part of this report we will review the formulation developed in Garrett.[3] As each term is discussed, the necessary integral will be developed and the results for a single Maxwellian presented for various temperatures and potentials. The final section will review the details of the two Maxwellian model and conclude with a comparison between theory and actual observations. These results indicate a standard deviation of ±1,200 V between observation and theory over the range -300 V to -10,000 V, while the region of applicability of the model is between +100 V and -20,000 V for potentials and between 10 eV and 50,000 keV for plasma temperatures – much larger than that of Garrett.[3]

2. GENERAL THEORY

The fundamental problem in determining the potential on a surface immersed in a plasma is the balance of currents leaving and striking the surface – an imbalance always results in a net addition or subtraction of charge, altering the potential until equilibrium is reached. In this study we will consider only the following currents for a single point (that is, leakage currents, capacitance, etc., are ignored):

$$J_E - (J_I + J_{SE} + J_{SI} + J_{BSE} + J_{PH}) = 0 \qquad (1)$$

where

J_E = incident electron current

J_I = incident ion current

J_{SE} = secondary emitted electron current due to J_E

J_{SI} = secondary emitted electron current due to J_I

J_{BSE} = backscattered electron current due to J_E

J_{PH} = photoelectron emission (independent of J_E or J_I)

Given the incident ion and electron spectra at the satellite surface, the currents J_E, J_I, J_{SE}, J_{SI}, and J_{BSE} (J_{PH} will be ignored in this study, though it is implicitly included in the model and can be readily modeled; see in particular

Garrett and DeForest[6]) are found and the potential ϕ on the spacecraft varied until Eq. (1) holds.

Subsequent sections will outline the procedure for calculating each of the currents in Eq. (1) as functions of N, the number density, T, the Maxwellian temperature, and ϕ, the satellite to space potential. We will in fact be dealing with the number flux, $\langle NF \rangle$, in units of particles/cm^2-sec-sr rather than the actual current density. For a truly omnidirectional flux they are related by:

$$J = q\pi\langle NF\rangle \tag{2}$$

where q = electronic charge.

Also we will be making the limiting assumption of a thick sheath surrounding the satellite. That is, we will assume that the distribution function $\tilde{f}$ at the surface of the spacecraft is related to the ambient distribution function f, for a Maxwellian distribution, by

$$\tilde{f}(E') = e^{-q\phi/KT} f(E') \tag{3}$$

where

$$f(E) = N(M/2\pi KT)^{3/2} e^{-E/KT}$$

and

K = Boltzmann's constant
M = mass
E = energy in ambient medium
E' = energy at surface

$$E = E' + q \cdot \phi \tag{4}$$

At geosynchronous orbit, the sheath (that is, the region over which particle orbits are distorted) is much larger than the spacecraft (typical values are 250 m for the sheath as compared with a few meters for the satellite) so that Eq. (3) is a good approximation. At lower altitudes (particularly in the plasmasphere) this relation breaks down and the detailed geometry of the satellite and its sheath must be considered.

---

6. Garrett, H.B. and DeForest, S.E. (1979a) Time-varying photoelectron flux effects on spacecraft potential at geosynchronous orbit, J. Geophys. Res. 84:283-2088.

3. ELECTRON AND ION INCIDENT CURRENT

In terms of the incident particle distribution, $\tilde{f}$, at the surface of the satellite, we can write the equations for the incident electron and ion currents as follows:*

$$J = \frac{2}{M^2} \int_0^\infty E\tilde{f}(E)\, dE \tag{5}$$

Substituting Eq. (3) for $\tilde{f}$, and remembering that the ambient particles do not have energies below 0, we find for the electrons:

$$J_E = \frac{2N_E}{M_E^2} \left(\frac{M_E}{2\pi T_E} \right)^{3/2} \int_x^\infty e^{-(E-\phi)/T_E} E\, dE \tag{6a}$$

For $\phi > 0$, $x = \phi$, implying:

$$J_E = K_E N_E T_E^{1/2} (1 + \phi/T_E) \tag{6b}$$

For $\phi \leq 0$, $x = 0$, implying:

$$J_E = K_E N_E T_E^{1/2} e^{(\phi/T_E)} \tag{6c}$$

where

M_E = mass of electron

N_E = number density of electrons in n/cm^3

T_E = electron temperature in eV

ϕ = satellite potential (in units of eV)

E = energy of electrons in eV

K_E = 5.326×10^6 for J_E in n/cm^2-sec-sr.

---

*Throughout, we are using the number flux in the equations even though we refer to it as the current – the two are related by Eq. (2). Also the units of charge q will be incorporated in ϕ, so that ϕ is in the units of eV rather than V (the sign of the charge will be explicit in each equation). T_E and T_I are assumed to include K, the Boltzmann constant.

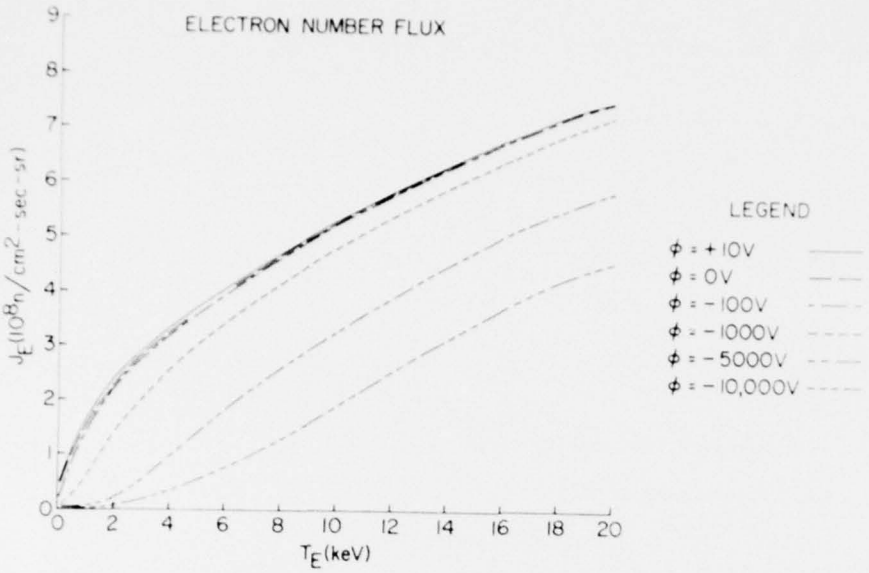

Figure 1a. Number Flux of Electrons (J_E) in Units of n/cm^2-sec-sr as a Function of Maxwell-Boltzmann Temperature (T_E) for Various Values of Satellite Potential (ϕ). N_E is assumed to be 1 cm^{-3}

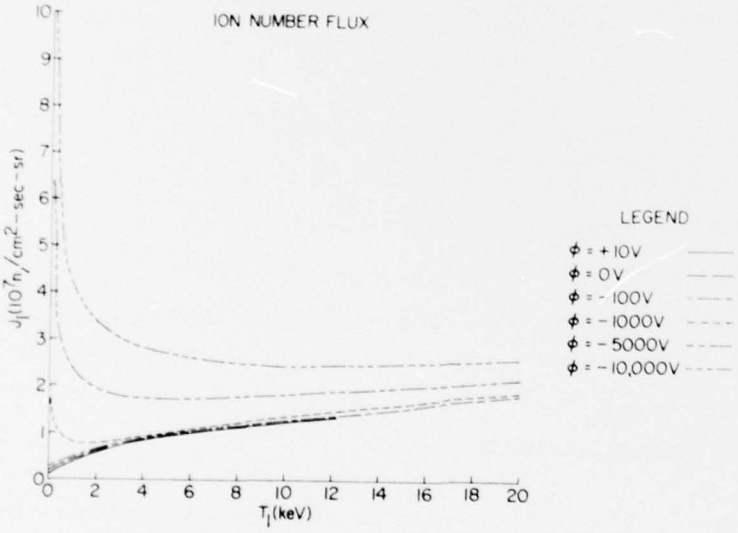

Figure 1b. Number Flux of Ions (J_I) in Units of n/cm^2-sec-sr as a Function of Maxwell-Boltzmann Temperature (T_I) for Various Values of Satellite Potential (ϕ). N_I is assumed to be 1 cm^{-3}

Similarly, for the ions (assumed to be protons):

For $\phi < 0$, $x = -\phi$, implying:

$$J_I = K_I N_I T_I^{1/2} (1 - \phi/T_I) \tag{7a}$$

For $\phi \geq 0$, $x = 0$, implying:

$$J_I = K_I N_I T_I^{1/2} e^{-\phi/T_I} \tag{7b}$$

where

N_I = number density of ions in n/cm^3

T_I = ion temperature in eV

$K_I = 1.2437 \times 10^5$ for J_I in n/cm^2-sec-sr.

Expressions (6) and (7) are plotted in Figure 1. As we shall see, they are of fundamental importance in many spacecraft charging applications and can be easily applied to calculate the current to the satellite due to the ambient environment for a plasma consisting of two or more components. As an example, for the case of a two-Maxwellian distribution of electrons and a negative potential:

$$J_E = K_E (N1E \cdot T1E^{1/2} e^{\phi/T1E} + N2E \cdot T2E^{1/2} e^{\phi/T2E}) \tag{8}$$

where

N1E = number density for electron component 1

T1E = temperature for electron component 1

N2E = number density for electron component 2

T2E = temperature for electron component 2

Similar equations follow for combinations of 3, 4, or higher sums of Maxwellian components.

4. SECONDARY EMISSION CURRENT

Secondary emission is the result of electrons being ejected from the satellite surface due to impinging electrons and ions (ion secondaries are not important). The secondary emission current is given by (remember, J_{SE} and J_{SI} are in units of n/cm^2-sec-sr):

$$J_{SE} = \frac{2}{M_I^2} \int_0^\infty \delta_E(E) \tilde{f}(E) E \, dE \tag{9}$$

$\delta_E(E)$, the secondary electron yield, is approximated for the electrons by:

$$\delta_E(E) = \begin{cases} \frac{C}{D} (\text{Log } E)^{\alpha-1} \cdot e^{-(\text{Log } E/\beta)} & \text{for } \phi < 0 \\ 0 & \text{for } E \leq 1 \text{ ev} \\ 0 & \text{for } \phi > 0 \end{cases} \tag{10}$$

where:

$\alpha = 10.8$

$\beta = 0.25$

$C = 1.8213$

$D = \beta^\alpha \Gamma(\alpha)$

$\Gamma(\alpha) = 2271560.4$

The function $\delta_E(E)$, for $\phi < 0$, has been plotted in Figure 2. It was chosen to be in close agreement with the secondary electron yield for electrons impacting on aluminum presented in Whipple.[4]

For electrons and $\phi < 0$, Eq. (9) becomes:

$$J_{SE} = \frac{2}{M_I^2} \int_x^\infty \delta_E(E) \tilde{f}_E(E) E \, dE$$

$$= \frac{K_E \cdot C}{D} \cdot \frac{N_E}{T_E^{3/2}} \cdot e^{\phi/T_E} \int_1^\infty e^{-(E/T_E + \text{Log } E/\beta)} (\text{Log } E)^{\alpha-1} E \, dE \tag{11}$$

The above integral cannot be integrated analytically. We have, however, integrated it numerically using the Gauss-Laguerre quadrature formulas. The results, normalized to $J_E(T_E, \phi)$, are plotted in Figure 3. It is clear from this figure that, for the range shown (namely, 10 eV < T_E < 100 keV and $0 < \phi < -10$ keV):

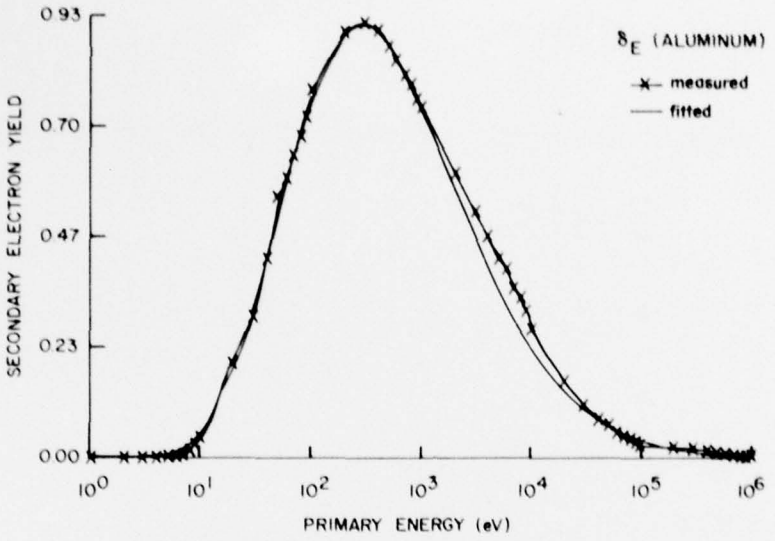

Figure 2. Plot of the Percentage of Electrons Returned as Secondaries Due to Electron Bombardment (δ_E) as a Function of Energy

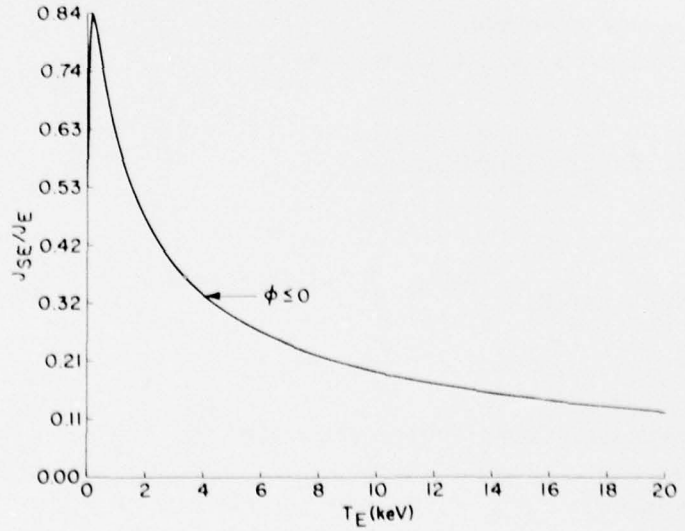

Figure 3. Ratio of Secondary Electron Number Flux Due to Electron Bombardment (J_{SE}) to Ambient Electron Number Flux at Surface (J_E) Versus Temperature (T_E) for Various Potentials

$$J_{SE}(T_E, \phi) \simeq J_E(T_E, \phi)\, S(T_E) \tag{12}$$

where

$$S(T_E) = \begin{cases} 0 & \phi > 0 \\ 0.843 - 0.842\, e^{-0.0286 T_E} & T_E \leq 200 \text{ eV} \quad \phi \leq 0 \\ 0.143 + 0.740\, e^{-0.0003 T_E} & T_E \geq 200 \text{ eV} \quad \phi \leq 0 \end{cases}$$

Although we have not used this expression in the model presented here, the gain in computation time from this latter expression should outweigh any loss in accuracy. As, however, we have sought accuracy in this study, we have in every case integrated Eq. (11) as indicated.

The expression for the secondary emission of electrons due to ions was taken to be:

$$\delta_I(E) = \begin{cases} K_2\, e^{-U/(E+V)} & \phi < 0 \quad E \geq R \\ K_1 & \phi < 0 \quad R > E \\ 0 & \phi > 0 \end{cases} \tag{13}$$

where

$K_1 = 0.086$, $K_2 = 5$

$U = 4060$, $V = 300$, $R = 700$

This is plotted in Figure 4 over a plot of $\delta_I(E)$ for aluminum taken from Whipple.[4] As the deviation above 100 keV is significant, we have limited our model to 50 keV (well above the region of naturally occurring charging phenomena), so the deviation is not of concern in our calculations.

Inserting Eq. (13) into Eq. (9) we find, for $\phi \leq 0$:

$$J_{SI} = \frac{2}{M_I^2} \int_{-\phi}^{\infty} \delta_I(E) \tilde{I}_I(E) E\, dE = \frac{K_I N_I}{T_I^{3/2}} \cdot e^{-\phi/T_I} \cdot$$

$$\cdot \left[K_1 \int_{-\phi}^{R} e^{-E/T_I} E\, dE + K_2 \int_{R}^{\infty} e^{-E/T_I} \cdot e^{-U/(E+V)} E\, dE \right] \tag{14}$$

where M_I is the mass of the ions.

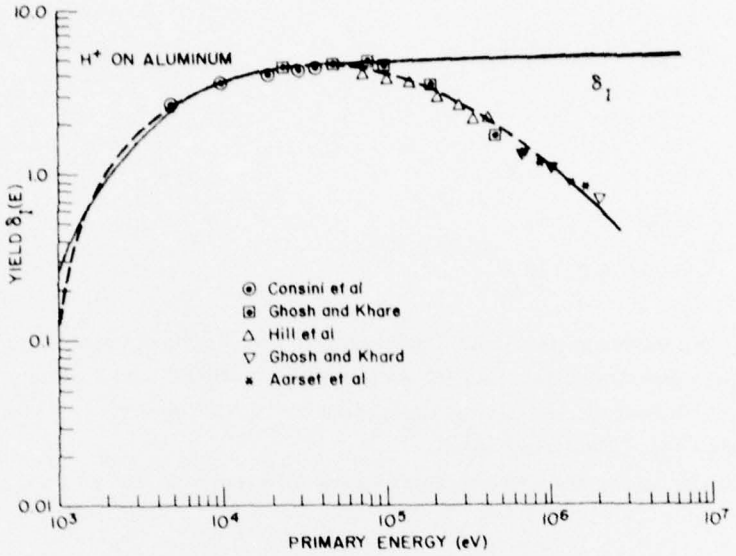

Figure 4. Plot of the Percentage of Electrons Returned as Secondaries Due to Ion Bombardment (δ_I) as a Function of Energy

Performing the above integrations and after some manipulations, we arrive at the form:

$$J_{SI} = -S1 \cdot e^{-(\phi+R)/T_I} + S2 \cdot (T_I - \phi) + S3 \cdot e^{-(\phi+R)/T_I} \int_0^\infty e^{-t} \cdot e^{-U/(t \cdot T_I + R + V)} (t \cdot T_I + R)\, dt \qquad (15)$$

where

$$S1 = KI \cdot K1 \cdot N_I \cdot (T_I + R)/(T_I)^{1/2}$$

$$S2 = KI \cdot K1 \cdot N_I/(T_I)^{1/2}$$

$$S3 = KI \cdot K2 \cdot N_I/(T_I)^{1/2}$$

Eq. (15) is integrated using the Gauss-Laguerre quadrature formulas. In Figure 5 we have plotted J_{SI}/J_I as a function of T_I and ϕ. Although not as simple as J_{SE}, we can again approximate these graphical results in an analytic form:*

$$J_{SI}(T_I, \phi) = J_I(T_I, \phi) \cdot W(T_I, \phi) \tag{16}$$

where:

$$W(T_I, \phi) = \begin{cases} 0 & \phi > 0 \\ (4.78 - 0.653\, e^{0.974\times10^{-4}\phi}) - (0.53 + 3.78\, e^{0.00018\phi}) \cdot \\ \cdot\ e^{-(0.572\times10^{-4} + 0.00018\, e^{0.00014\phi})T_I} & \phi \le 0 \ ; \end{cases}$$

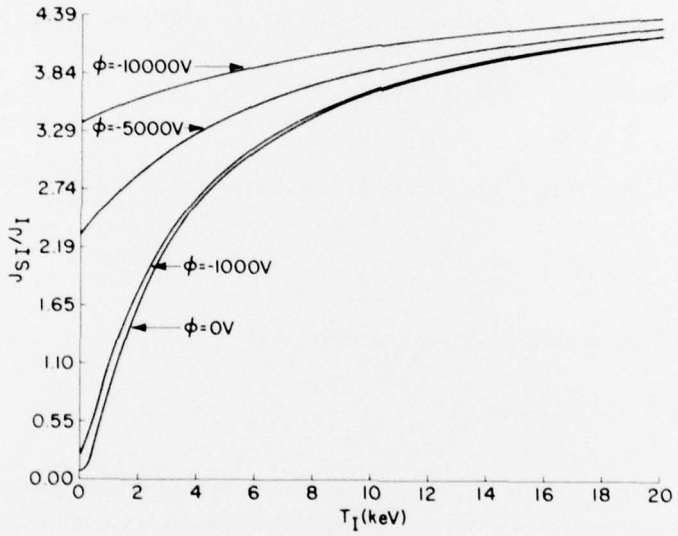

Figure 5. Ratio of Secondary Electron Number Flux Due to Ion Bombardment (J_{SI}) to Ambient Ion Number Flux at Surface (J_I) Versus Temperature (T_I) for Various Potentials

*Eq. (16) can give negative values as it is only an approximation. These values should be set equal to 0.

5. BACKSCATTERED ELECTRON CURRENT

As implied in its name, the backscattered current is the result of the backscattering or reflection of the incident particles. It is, for our calculations, only a significant factor for electrons. The basic equation is:

$$J_{BSE} = \frac{2}{M_E^2} \int_x^\infty dE' \int_{E'}^\infty B(E', E)\tilde{f}_E(E)E\, dE \tag{17}$$

where

$$x = \begin{cases} 0 & \text{if } \phi < 0 \\ \phi & \text{if } \phi > 0 \end{cases}$$

$B(E', E)$ = percentage of electrons scattered at a given energy E' as a result of an incident electron at energy E.

E' = energy of backscattered particles ($E' \leq E$)

E = energy of incident particles

Following Sternglass,[7] $B(E', E)$ is usually given in the normalized form:

$$B(E', E) = \frac{G(E'/E)}{E} \tag{18}$$

G is given as a function of E'/E for aluminum by:

$$G(E'/E) \simeq \frac{4}{3}(E'/E)(1 - E'/E) \tag{19}$$

We obtained Eq. (19) from an approximate fit to Sternglass[7] and DeForest (private communication, see Garrett[3]). Substituting into Eq. (17):

For $\phi \leq 0$:

$$J_{BSE} = P1 \cdot e^{\phi/T_E} \tag{20a}$$

---

7. Sternglass, E.J. (1954) Backscattering of kilovolt electrons from solids, Phys. Res. 95:345.

For $\phi \geq 0$:

$$J_{BSE} = L1 \cdot (1 + \phi/T_E) + L2 \cdot \phi^2 - L3 \cdot \phi^2 \cdot (3 + 2\phi/T_E) \cdot$$

$$\cdot \int_0^\infty \frac{e^{-y}}{(y + \phi/T_E)}\, dy \qquad (20b)$$

where:

$$P1 = \frac{2}{9} N_E T_E^{1/2}$$

$$L1 = \frac{2}{9} N_E T_E^{1/2}$$

$$L2 = \frac{4}{9} \frac{N}{T_E^{3/2}}$$

$$L3 = \frac{2}{9} \frac{N}{T_E^{3/2}}$$

The integration is performed by the Gauss-Laguerre quadrature formula. The results, normalized by $J_E(\phi, T_E)$, are plotted in Figure 6. The detailed numerical integral results in Figure 6 can be roughly fitted by:

$$J_{BSE} = BS(\phi, T_E) \cdot J_E(\phi, T_E) \qquad (21)$$

where

$$BS(\phi, T_E) = \begin{cases} \frac{2}{9} & \phi \leq 0 \\ (0.253 - 0.0027\, e^{0.072\phi}) + (0.0867 + 0.657\, e^{-0.184\phi}) \cdot & \\ \cdot\ e^{-(0.00017 + 0.0098\, e^{-0.231\phi})\, T_E} & \phi > 0 \end{cases}$$

As before, the actual integral was used for the calculation.

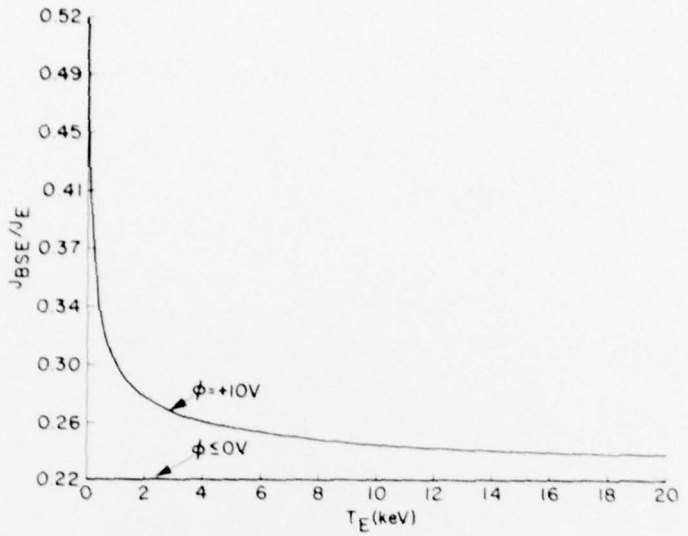

Figure 6. Ratio of Backscattered Electron Number Flux Due to Electron Bombardment (J_{BSE}) to Ambient Electron Number Flux at Surface (J_E) Versus Temperature (T_E) for Various Potentials

6. TWO MAXWELLIAN MODEL

As discussed in the Introduction, Garrett[1] and Garrett and DeForest[2] have presented evidence that, at least for the energy range ~ 10 eV to ~ 100 keV, the plasma population can be adequately represented by a sum of two Maxwellian components for both the electrons and ions. Experience shows this to be true for approximately 80 percent of the cases. Although more components would naturally give a better fit, and in about 10 percent of the cases a single Maxwellian is adequate, a two Maxwellian approximation is a very convenient way to represent the plasma as it can be directly derived from the first four moments of the distribution function. These four moments (see Garrett[1]) are the quantities most often provided by particle experiments, and hence most readily available. With these factors in mind, our charging model was designed to be optimized for two Maxwellian distributions.

Eq. (1) becomes:

$$[J_E(\phi, N1E, T1E) + J_E(\phi, N2E, T2E)] - \{[J_I(\phi, N1I, T1I) + J_I(\phi, N2I, T2I)]$$

$$+ [J_{SE}(\phi, N1E, T1E) + J_{SE}(\phi, N2E, T2E)] + [J_{SI}(\phi, N1I, T1I) + J_{SI}(\phi, N2I, T2I)]$$

$$+ [J_{BSE}(\phi, N1E, T1E) + J_{BSE}(\phi, N2E, T2E)] + J_{PH}(\phi)\} = 0 \qquad (22)$$

where:

N1E, T1E = Maxwellian number density and temperature for electron component 1

N2E, T2E = Maxwellian number density and temperature for electron component 2

N1I, T1I = Maxwellian number density and temperature for ion component 1

N2I, T2I = Maxwellian number density and temperature for ion component 2

J_E = incident electron current given by Eq. (6)

J_I = incident ion current given by Eq. (7)

J_{SE} = secondary electron current given by Eq. (11)

J_{SI} = secondary ion current given by Eq. (15)

J_{BSE} = backscattered electron current given by Eq. (21)

J_{PH} = photoelectron current, assumed zero in this paper (see Garrett,[3] however)

Eq. (22) is solved by substituting values of ϕ until it is satisfied, a process for which a variety of schemes can be employed. In this study, ϕ was steadily decreased in coarse steps until Eq. (22) became negative. At this point, the interval bracketed by this value and the preceding value was subdivided into finer intervals and the process iterated until a close approximation to zero was found.

Before analyzing the results of our model, one final point remains to be discussed concerning the adequacy of our assumptions. The assumption of a thick sheath, or, equivalently, assuming the satellite to be a point, limits the accuracy of our results as the sheath can alter the ambient plasma to a significant degree before the plasma strikes the satellite. This assumption, however, is not serious in comparison with that of assuming the satellite to be made uniformly of aluminum. First, the material properties (that is, δ and B) are at best only qualitatively understood. Secondly, it is obvious that few satellites consist of aluminum.

In fact, the two geosynchronous satellites ATS-5 and ATS-6 considered in this study consisted of a variety of materials. In order to compensate for this, *in Garrett*[3] a careful analysis was carried out in order to study the effects of varying δ and B. It was found adequate to multiply these factors by a constant of the order of unity to bring the results for ATS-5 and ATS-6 into agreement with observations. The correction factors adopted for this study, based on ATS-5, were:

$$\begin{aligned} \tilde{\delta}_E &= 1.3\ \delta_E \\ \tilde{\delta}_I &= 0.55\ \delta_I \\ \tilde{B}(E', E) &= 0.4\ B(E', E) \end{aligned} \tag{23}$$

The ATS-6 values were different, but as we are interested in a "universal" model we will employ the ATS-5 values throughout as representative.

7. DATA ANALYSIS

ATS-5 and ATS-6 are both geosynchronous satellites. We have integrated the digital data from the University of California plasma detectors on these two satellites to obtain the four plasma moments (for the energy ranges 50 eV to 50 keV and 0 to 80 keV, respectively) for the ambient environment. To be precise, the ambient environment immediately preceding eclipse entry (or following eclipse exit) and immediately after exit (or immediately preceding exit) from eclipse was computed, the results being corrected for satellite potential. The corresponding eclipse potentials were also computed. The two Maxwellian components where possible (if not, a single Maxwellian was chosen) were computed. These values and their averages (giving three sets of 23 values each) were employing the model as just outlined, used to compute the potentials for the sunlit, eclipsed, and average test cases. The three sets of estimated potentials are plotted versus the observed potentials in Figures 7a, 7b, and 7c. Although there is obvious agreement between the observed and predicted potentials in these figures, we will demonstrate mathematically their agreement in the subsequent paragraphs (see Table 1).

Table 1. Statistical Analysis of ATS-5 and ATS-6 Eclipse Data

	Number of Points 23 Degrees of Freedom 21							
							$\alpha = 0.05$	
	A	B	S_A	S_B	σ	r	H0: A = 0 H1: A ≠ 0	H0: B = 1 H1: B ≠ 1
First* Set	202.60	0.714	412.30	0.107	1179.71	0.82	Accept H0	Reject H0
Second Set	538.33	1.052	400.42	0.104	1145.72	0.91	Accept H0	Accept H0
Third Set	-295.85	1.179	450.55	0.117	1289.17	0.91	Accept H0	Accept H0

*The first set is for sunlit data, eclipse data make up the second set, and the third set is an average of the two.

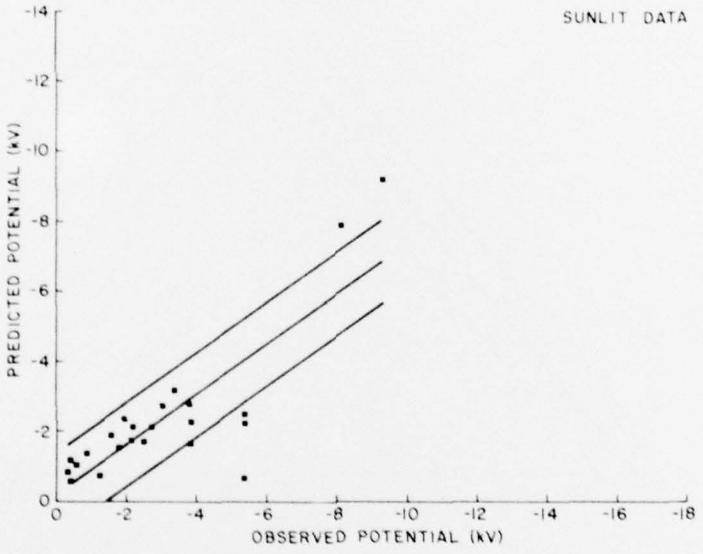

a. Sunlit Data

Figure 7. Observed Versus Predicted Potentials for ATS-5 and ATS-6 for Three Sets of Estimates of the Ambient Environment – Sunlit Conditions, Eclipse Conditions, and the Average of These Two Estimates

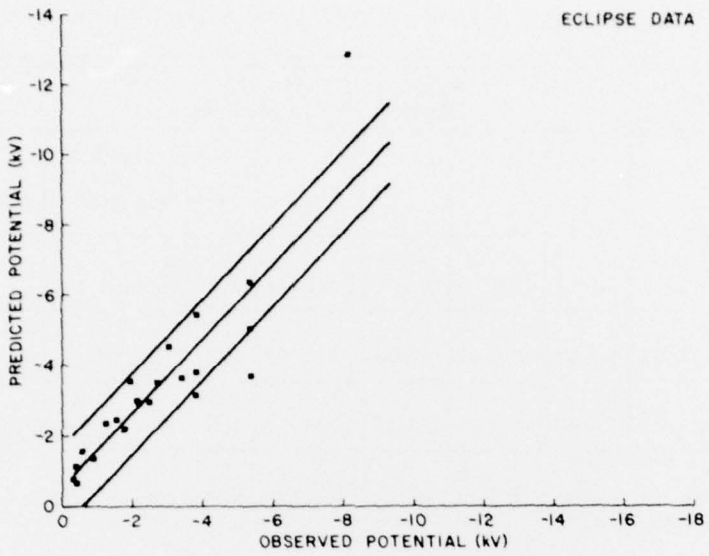

b. Eclipse Data

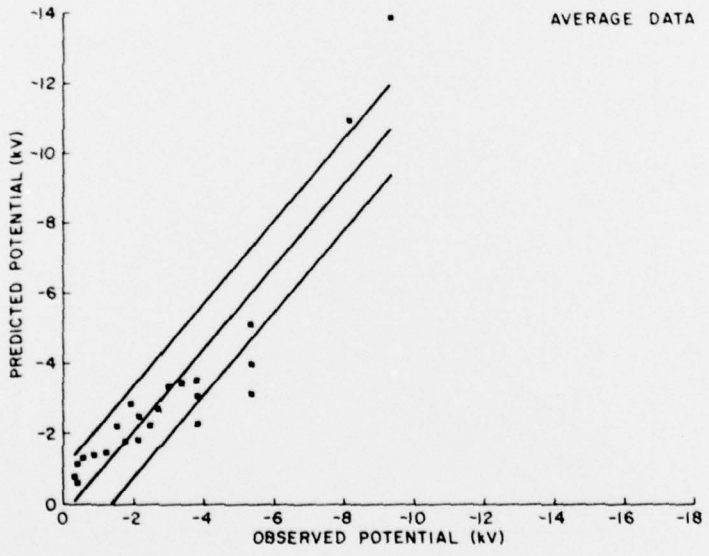

c. Average Data

Figure 7. Observed Versus Predicted Potentials for ATS-5 and ATS-6 for Three Sets of Estimates of the Ambient Environment – Sunlit Conditions, Eclipse Conditions, and the Average of These Two Estimates (Continued)

8. STATISTICAL ANALYSIS

If there is a relationship between the experimental and theoretical values of the potential, the simplest model should be a straight line relation of the form

$$Y = A + BX \tag{24}$$

where X signifies the experimental values and Y the theoretical values of the potential. For perfect agreement between X and Y we should have A = 0 and B = 1.

Three sets of data, each having 23 points, have been obtained and each set has been studied statistically. For the first set, the least squares estimates b and a of B and A, respectively, are found to be

$$b = 0.714 \quad \text{and} \quad a = 202.60 \ .$$

To create a confidence interval for A, we choose $\alpha = 0.05$ as the level of significance, and we conclude that a 95 percent confidence interval for A is

$$M1 < A < M2$$

with $M1 = a - S_A t_{0.025}$ and $M2 = a + S_A t_{0.025}$ being the lower and upper confidence limits, respectively. For the data, these were found to be M1 = -654.98 and M2 = 1060.18. This shows that 95 percent of the time the mean A of the Y- intercept of the straight line (24) will fall inside the above confidence interval. In other words, the confidence interval would contain the parameter A of the population with a probability of 95 percent.

As mentioned before, to have a perfect relationship between X and Y we should have A = 0 and B = 1. Now, the question is asked, is it logical to consider the value of A to be zero or not? For this we test the null hypothesis H0: A = 0, against the alternative H1: A $\neq$ 0. Here we consider a two-tailed critical region for $\alpha = 0.05$ level of significance. The region of acceptance would be all values of a such that

$$PR\left[-t_{\alpha/2} < \frac{a - A}{S_A} < t_{\alpha/2}\right] = 0.95$$

or

$$PR\left[A - S_A t_{\alpha/2} < a < A + S_A t_{\alpha/2}\right] = 0.95$$

We will accept the hypothesis if the estimated value a of A is inside the region of acceptance and reject it if it is in the critical region. For A = 0 the region of acceptance becomes

$$-857.58 < a < 857.58 \ .$$

Since a = 202.60, it falls inside the acceptance region and the null hypothesis (A = 0) is accepted. This procedure guarantees that the probability of rejecting the hypothesis A = 0 when it is in fact true is less than $\alpha = 0.05$. In addition, this procedure guarantees the probability of accepting A = 0 when it is not true is smaller than in any other test with the same α. (This is the so-called uniformly most powerful test when the alternative hypothesis is $A \neq 0$).

A similar situation prevails for the slope B of the line (24). A $(1 - \alpha)100\%$ confidence interval for the parameter B is given by the double inequality

$$b - S_B t_{\alpha/2} < B < b + S_B t_{\alpha/2}$$

which means that

$$PR\left[b - S_B t_{\alpha/2} < B < b + S_B t_{\alpha/2}\right] = 1 - \alpha$$

Choosing, as before, $\alpha = 0.05$ as the level of significance, we obtain the following confidence interval for B:

$$N1 < B < N2$$

where N1 = 0.49 and N2 = 0.94. This shows that 95 percent of the time the slope B of the straight line (24) would be between N1 and N2.

Now testing the hypothesis H0: B = 1 against the alternative H1: $B \neq 1$ we consider, as before, a two-tailed critical region for $\alpha = 0.05$ level of significance. The region of acceptance would be all values of b such that

$$PR\left[-t_{\alpha/2} < \frac{b - B}{S_B} < t_{\alpha/2}\right] = 0.95$$

or all values of b which satisfy the double inequality

$$K1 < b < K2$$

where $K1 = B - S_B t_{\alpha/2}$ and $K2 = B + S_B t_{\alpha/2}$.

In the present case, K1 = 0.777, K2 = 1.223, and b = 0.714. It appears that in this case the null hypothesis B = 1 is not consistent with the data, and thus our best estimate (minimum variance) would be B = 0.714. However, it should be noted that for a level of significance $\alpha = 0.01$ considering a critical region outside of the interval

$$0.697 < B < 1.3029$$

the hypothesis B = 1 is accepted.

Table 1 gives a general picture of the statistical analysis done for all three sets of data. The letter A signifies the Y-intercept of the line (24), B denotes the slope, and S_A and S_B represent the standard deviations of A and B, respectively. H0 denotes the null hypothesis, H1 the alternative hypothesis. The standard error is denoted by σ and the correlation coefficient is denoted by r. Based on this table, it appears that to a reasonable degree of accuracy (±1, 200 V), our model based on a two-Maxwellian approximation and a simple material configuration predicts spacecraft potentials in eclipse.

9. CONCLUSION

In the preceding sections we have outlined a procedure for taking a two-Maxwellian distribution (or, for that matter, any number of Maxwellian distributions) and computing the potential difference between a shadowed satellite surface and the ambient environment. Our results indicate an accuracy (actually the standard error between the observed and predicted potentials) of ±1, 200 V. This is to be compared with the "exact" calculation using the detailed distribution function of Garrett[3] for which an error of ±700 V was reported and that of Garrett et al[8] for the crude estimate of $\phi \approx -T_E \text{ Ln } (J_E/10J_I)$ of ±2, 000 V. As the range of accuracy of the representation of the distribution function and current balance decreases from Garrett[3] to this paper to Garrett et al, [8] this trend is in good agreement with expectations.

The power of the techniques presented in this paper, however, is not the accuracy (which can be improved by "tuning" the model as discussed in Garrett[3]) but in the possibility of deriving an efficient, analytic expression for the potential. This is evident in Eqs. (6), (7), (12), (16), and (21). Multiple Maxwellian

8. Garrett, H.B., Rubin, A.G., and Pike, C.P. (1979) Prediction of Spacecraft Potentials at Geosynchronous Orbit, (edited by D.F. Donnelly) to appear in Proceedings of the Solar-Terrestrial Predictions Workship.

distributions can be easily incorporated using these equations in a straightforward fashion. We intend to pursue this formulation in subsequent papers, leading ultimately to a simple method of deriving spacecraft to space potentials.

References

1. Garrett, H.B. (1977) Modeling of the Geosynchronous Orbit Plasma Environment – Part I, AFGL-TR-77-0288, AD A053 164.
2. Garrett, H.B. and DeForest, S.E. (1979b) An analytical simulation of the geosynchronous plasma environment, to appear in Planet. Space Sci.
3. Garrett, H.B. (1978) Spacecraft Potential Calculations – A Model, AFGL-TR-78-0116, AF Surveys in Geophysics, No. 387, AD A060 151.
4. Whipple, E.C. (1965) The Equilibrium Electric Potential of a Body in the Upper Atmosphere, NASA X-615-65-296.
5. DeForest, S.E. (1972) Spacecraft charging at synchronous orbit, J. Geophys. Res. 27:651.
6. Garrett, H.B. and DeForest, S.E. (1979a) Time-varying photoelectron flux effects on spacecraft potential at geosynchronous orbit, J. Geophys. Res. 84:283-2088.
7. Sternglass, E.J. (1954) Backscattering of kilovolt electrons from solids, Phys. Res. 95:345.
8. Garrett, H.B., Rubin, A.G., and Pike, C.P. (1979) Prediction of Spacecraft Potentials at Geosynchronous Orbit, (edited by D. F. Donnelly) to appear in Proceedings of the Solar-Terrestrial Predictions Workshop.